Analysis of the Electrolyte Convection inside the Concentration Boundary Layer during Structured Electrodeposition of Copper in High Magnetic Gradient Fields

ARTICLE *in* ANALYTICAL CHEMISTRY · MARCH 2013

Impact Factor: 5.64 · DOI: 10.1021/ac302601t · Source: PubMed

5 AUTHORS, INCLUDING:

Jörg König
Technische Universität Dresden
21 PUBLICATIONS **69** CITATIONS
SEE PROFILE

Kristina Tschulik
Ruhr-Universität Bochum
96 PUBLICATIONS **705** CITATIONS
SEE PROFILE

Margitta Uhlemann
Leibniz Institute for Solid State and Materials …
105 PUBLICATIONS **1,521** CITATIONS
SEE PROFILE

Jürgen Czarske
Technische Universität Dresden
267 PUBLICATIONS **1,187** CITATIONS
SEE PROFILE

analytical chemistry

Article

pubs.acs.org/ac

Analysis of the Electrolyte Convection inside the Concentration Boundary Layer during Structured Electrodeposition of Copper in High Magnetic Gradient Fields

Jörg König,*[,†] Kristina Tschulik,*[,‡] Lars Büttner,[†] Margitta Uhlemann,[‡] and Jürgen Czarske[†]

[†]Faculty of Electrical Engineering and Computer Engineering, Laboratory for Measurement and Testing Techniques, Technische Universität Dresden, Helmholtzstrasse 18, 01069 Dresden, Germany

[‡]Institute for Complex Materials, IFW Dresden, P.O. 270116, 01171 Dresden, Germany

ABSTRACT: To experimentally reveal the correlation between electrodeposited structure and electrolyte convection induced inside the concentration boundary layer, a highly inhomogeneous magnetic field, generated by a magnetized Fe-wire, has been applied to an electrochemical system. The influence of Lorentz and magnetic field gradient force to the local transport phenomena of copper ions has been studied using a novel two-component laser Doppler velocity profile sensor. With this sensor, the electrolyte convection within 500 μm of a horizontally aligned cathode is presented. The electrode-normal two-component velocity profiles below the electrodeposited structure show that electrolyte convection is induced and directed toward the rim of the Fe-wire. The measured deposited structure directly correlates to the observed boundary layer flow. As the local concentration of Cu^{2+} ions is enhanced due to the induced convection, maximum deposit thicknesses can be found at the rim of the Fe-wire. Furthermore, a complex boundary layer flow structure was determined, indicating that electrolyte convection of second order is induced. Moreover, the Lorentz force-driven convection rapidly vanishes, while the electrolyte convection induced by the magnetic field gradient force is preserved much longer. The progress for research is the first direct experimental proof of the electrolyte convection inside the concentration boundary layer that correlates to the deposited structure and reveals that the magnetic field gradient force is responsible for the observed structuring effect.

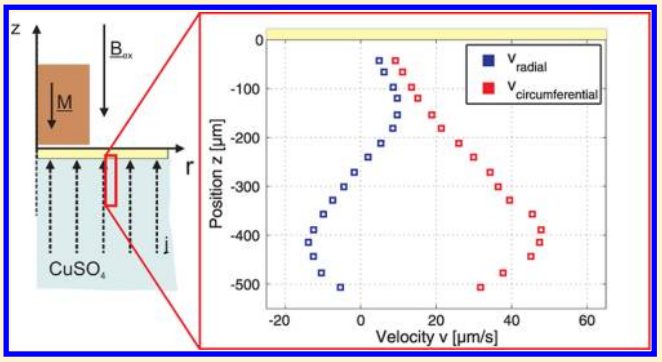

The application of magnetic gradient fields to electrochemical processes has been investigated intensively in the past few years. Beside their application for magnetohydrodynamic (MHD)-pumping[1,2] and their effects on redox processes,[3,4] the impact of magnetic gradients on electrodeposition has been of major research interest. Comprehensive studies were performed from both the numerical and experimental side.[5−10] As observed, structured metal layers are obtained when paramagnetic ions, e.g., Cu^{2+} ions, are involved. Furthermore, the deposited structure directly correlates to the distribution of the magnetic gradient fields applied. This suggests that the magnetic field gradient force ($\mathbf{f}_{VB}$) affects the deposition process by inducing a convection of the electrolyte toward high $(\mathbf{B}\cdot\nabla)\,\mathbf{B}$. However, by applying external magnetic fields to the electrodeposition process, competing forces, e.g., the Lorentz force ($\mathbf{f}_L$) and the buoyant force ($\mathbf{f}_G$), are usually involved. These forces can induce additional convection of the electrolyte influencing the near-electrode distribution of the electroactive species as well. Thereby, the most distinctive effects are expected inside the concentration boundary layer. Hence, measuring the electrolyte convection in the direct vicinity of the electrode provides information about the correlation between acting forces and the resulting structured deposit. Recently, the electrolyte convection at high magnetic gradient fields has been examined using the astigmatism microparticle tracking velocimetry (μPTV).[8] Even though the measurement inside the electrolytic cell succeeded and the results show a convection induced by the magnetic field gradient force that protrudes up to the bulk electrolyte, spatially resolved velocity information inside the concentration boundary layer is still missing. The velocities in the vicinity of the electrode were averaged over a distance of up to 4 mm, i.e., several times larger than the thickness of the concentration boundary layer. With a typical thickness of the concentration boundary layer in the range of 10^{-4} to 10^{-3} m,[11] the measurements are only partially suitable to show, in detail, the correlation between the near-electrode distribution of the Cu^{2+} ions caused by induced electrolyte convection and the deposited structure.

To have a specifically structured pattern, well-defined (inhomogeneous) magnetic fields have to be superimposed. This has usually been realized using magnet arrays or

Received: September 8, 2012
Accepted: February 23, 2013
Published: February 23, 2013

magnetized ferromagnetic templates with small dimensions.[5,10] For example, considering the simplified configuration depicted in Figure 1, a strong magnetic gradient field is generated in front of the cathode by placing a thin Fe-wire, which is magnetized by a magnetic field $\mathbf{B}_{ex}$, directly behind the electrode. Due to the downward-facing cathode, natural convection can be neglected, as the depleted and thus lighter solution is always on top. Hence, only the influences of the magnetic field gradient force and the Lorentz force have to be considered in this configuration.

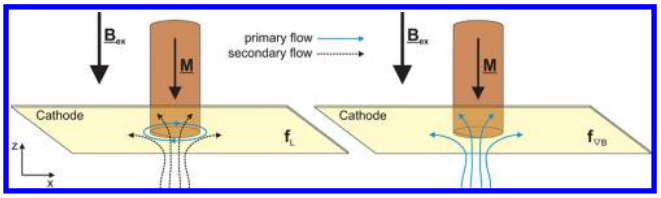

Figure 1. Sketch of the near-electrode convection induced by the Lorentz force (left) and the magnetic field gradient force (right) in front of a downward-facing cathode, when a magnetized Fe-wire is placed behind the electrode.

The Lorentz force density $\mathbf{f}_L = \mathbf{j} \times \mathbf{B}$ is given by the cross product of the current density $\mathbf{j}$ and the magnetic flux density $\mathbf{B}$. In case of an inhomogeneous magnetic field of cylindrical symmetry, as caused by the magnetized Fe-wire in Figure 1, the Lorentz force density reads

$$\mathbf{f}_L = j_z B_r \mathbf{e}_\phi \tag{1}$$

and depends on the radial magnetic flux density B_r and the axial current density j_z . The $\mathbf{e}_\phi$ denotes the unity vector in azimuthal direction. Hence, as indicated in the left part of Figure 1, the Lorentz force-driven convection stirs primarily azimuthally. However, centrifugal forces induce a secondary flow that transports the electrolyte outward. Due to continuity, an electrode-normal convection arises that continuously transports Cu^{2+}-rich bulk electrolyte toward the cathode and enhances, therefore, the local mass transport near the Fe-wire.

In contrast to the Lorentz force, the magnetic field gradient force only occurs in magnetic gradient fields and reads[7]

$$\mathbf{f}_{\nabla \mathbf{B}} = \frac{\chi_{sol}}{\mu_0}(\mathbf{B}\cdot\nabla)\mathbf{B} \tag{2}$$

Hereby, the χ_{sol} denotes the total magnetic susceptibility of the electrolyte, and μ_0 is the vacuum permeability. Taking the curl of $\mathbf{f}_{\nabla \mathbf{B}}$ into account, the impact of the magnetic field gradient force has to be distinguished in two local regions.[7]

$$\nabla \times \mathbf{f}_{\nabla \mathbf{B}} = \frac{\chi_m}{2\mu_0}(\nabla c) \times (\nabla B^2) \tag{3}$$

Here, χ_m denotes the molar susceptibility of Cu^{2+} ions only and c their concentration. In the bulk solution, where an ion concentration gradient is nonexistent, the $\nabla \times \mathbf{f}_{\nabla \mathbf{B}}$ is conservative, meaning that no flow is induced as potential forces are balanced by wall pressure in closed geometries.[7] However, inside the concentration boundary layer, where the concentration gradient can be very large, the magnetic field gradient force is able to induce a flow.

Considering again the simplified configuration of a single magnetized Fe-wire and assuming a magnetic field consisting only of radial and axial components, the curl of the magnetic field gradient force holds[7]

$$\nabla \times \mathbf{f}_{\nabla \mathbf{B}} = \frac{\chi_m}{\mu_0}\frac{\Delta c}{\delta_c} B \frac{\partial B}{\partial r}\mathbf{e}_\phi \tag{4}$$

and induces an electrolyte convection particularly toward regions of maximum gradients. These maximum gradients are located at the rim position of the Fe-wire.[5,7,8] Hence, as indicated in the right part of Figure 1, the supposed near-electrode convection induced by the magnetic field gradient force is very similar to the secondary flow caused by the Lorentz force.[7] As depicted in Figure 2, a dull ring onto the cathode surface is obtained, when a small magnetized Fe-wire is placed behind the cathode. Either the secondary flow induced by the Lorentz force or the convection induced by the magnetic field gradient force significantly influence the deposition process by transporting Cu^{2+} ions toward the rim position of the Fe-wire. The topography of the copper deposit confirms that the mass transport near the rim is enhanced, because maximum deposit thicknesses are found there.

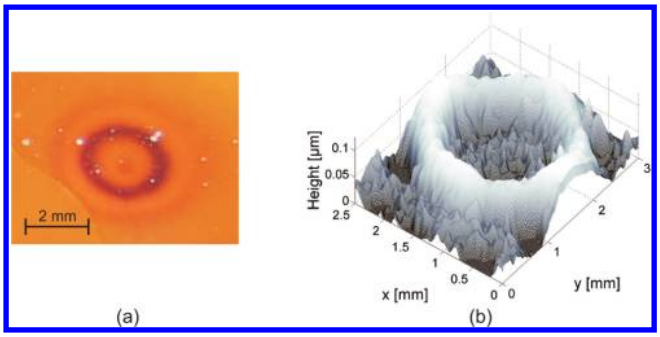

Figure 2. (a) Picture and (b) topography of the Cu deposit obtained after a deposition of 10 min duration (concentration c_0 = 5 mM).

In eq 4, Δc represents the concentration gradient in electrode-normal direction inside the concentration boundary layer of thickness δ_c. The thickness of δ_c can be derived applying Fick's first law.[12] In advance to the present experiment, the estimated average concentration boundary layer thickness amounts to either $\delta_c \approx 371\ \mu m$ or $\delta_c \approx 439\ \mu m$, depending on the Cu^{2+} concentration applied and the actual average limiting current density measured. (Diffusion coefficient:[13] $D = 0.714 \times 10^{-5}$ cm^2/s, measured average limiting current densities: $\overline{j}$(@ 5 mM) ≈ -0.134 A/cm^2, $\overline{j}$(@ 10 mM) ≈ -0.226 A/cm^2.) This relatively thin concentration boundary layer emphasizes the challenging measurement task. To assess the contribution of the Lorentz and the magnetic field gradient force to the structured electrodeposition process, spatially resolved velocity measurements within this distance are of vital importance. The present work aims to provide these measurements.

EXPERIMENTAL SECTION

Experimental Setup. A sketch of the experimental setup is depicted in Figure 3. The cylindrical electrochemical cell was made of poly(methyl methacrylate) (PMMA) with an inner diameter of 13 mm in width. The total (inner) height of the cell amounted to 15 mm. The working electrode (WE) at the top of the cell consisted of a thin glass disk (70 μm in thickness, electrode surface 1.33 cm^2) evaporated with a Au-layer of 200 nm in thickness. To superimpose a high magnetic gradient field

dx.doi.org/10.1021/ac302601t | Anal. Chem. 2013, 85, 3087−3094

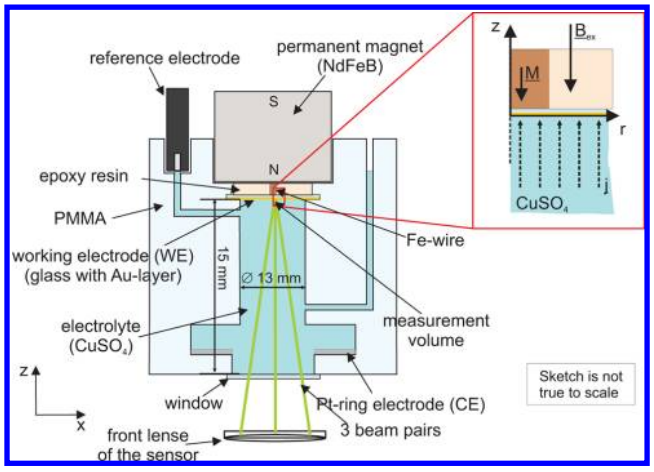

Figure 3. Sketch of the experimental setup with the LDV-PS (indicated by the front lens). The three beam pairs of the sensor intersect in front of the cathode and shape the measurement volume, which contains the three superimposed interference fringe systems.

at the WE, a centrally located single Fe-wire (d = 2 mm, l = 7 mm), magnetized by a neodymium−iron−boron (NdFeB) permanent magnet (25 mm in diameter and 15 mm in length, magnetic flux density at the surface of about 0.45 T), was placed directly behind the WE. A saturated reference electrode (mercury/mercurous sulfate electrode (MSE)) was situated near the WE via a capillary (d = 1 mm). A window at the bottom of the cell enabled optical observation of the velocity distribution inside the concentration boundary layer at the WE through measurement of the entire 15 mm-high cell. For that reason, a Pt-ring electrode served as a counter electrode (CE). Due to the large distance of 14 mm between CE and WE as well as due to the focus on the velocity distribution being within approximately 500 μm of the front of the WE, a homogeneous current distribution that is almost perfectly perpendicular to the WE at the measurement region is assumed. Thus, no effects due to bent current lines are expected that might affect additionally the resulting electrolyte convection inside the concentration boundary layer. In addition, the horizontally aligned WE at the top of the electrochemical cell avoids natural convection. In contrast to the measurements performed in ref 8, this setup allows detailed investigations of the convections induced by the Lorentz and magnetic field gradient force without any side effects caused by buoyancy. All measurements were performed during diffusion-controlled deposition. A potential of E = −800 mV vs MSE was set by a single step for the potentiostatic deposition experiments with a Jaissle potentiostat in a three-electrode arrangement. According to ref 6, this potential allows for diffusion-controlled deposition of Cu, i.e., for a well-established concentration gradient near the WE. The electrolytes used for the experiments were an aqueous solution of 5 mM or 10 mM $CuSO_4$, and 0.105 or 0.1 M Na_2SO_4 as supporting electrolyte, respectively. To adjust the pH value to 3.0, H_2SO_4 was added to the electrolyte. All measurements were conducted at a room temperature of 23 °C.

Measurement Technique. The electrolyte convection during the structured deposition has been measured employing a laser Doppler velocity profile sensor (LDV-PS) utilizing time division multiplexing (TDM).[14,15] Its unique feature of high spatial resolution down to the micrometer level, despite a long working distance (>50 mm), allows for observing small scale flow phenomena in comparably large environments. In conjunction with fluorescent tracer particles, to suppress unwanted reflections from the electrode surface, this sensor fulfills the essential requirements for spatially resolved velocity measurements inside the concentration boundary layer.

The LDV-PS poses an extension of the standard laser Doppler velocimetry (LDV) and enables the simultaneous measurement of velocity and tracer particle position as follows. The sensor features two fan-like interference fringe systems, one diverging and one converging along the optical z-axis. Both are superimposed in a common measurement volume. When a tracer particle, which is seeded to the fluid (electrolyte), passes through the measurement volume, it coincidentally scatters light from both interference fringe systems. The scattered light is modulated by the respective Doppler frequencies f_1 and f_2. These Doppler frequencies depend on the local fringe spacing,

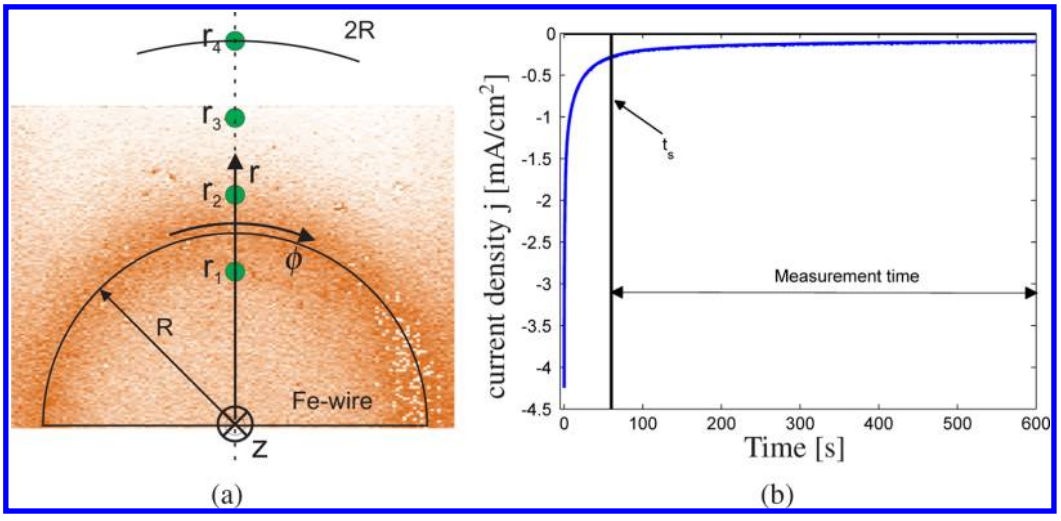

Figure 4. (a) Top view of the cathode surface with the four different measurement positions along the centerline of the Fe-wire placed directly behind the working electrode. At each measurement position, the radial as well as the circumferential velocity component of the electrolyte convection are measured along the electrode-normal direction. The color displays the deposited ring structure onto the cathode surface. (b) Recorded current density j during electrolysis. t_s is the starting measurement time.

dx.doi.org/10.1021/ac302601t | Anal. Chem. 2013, 85, 3087−3094

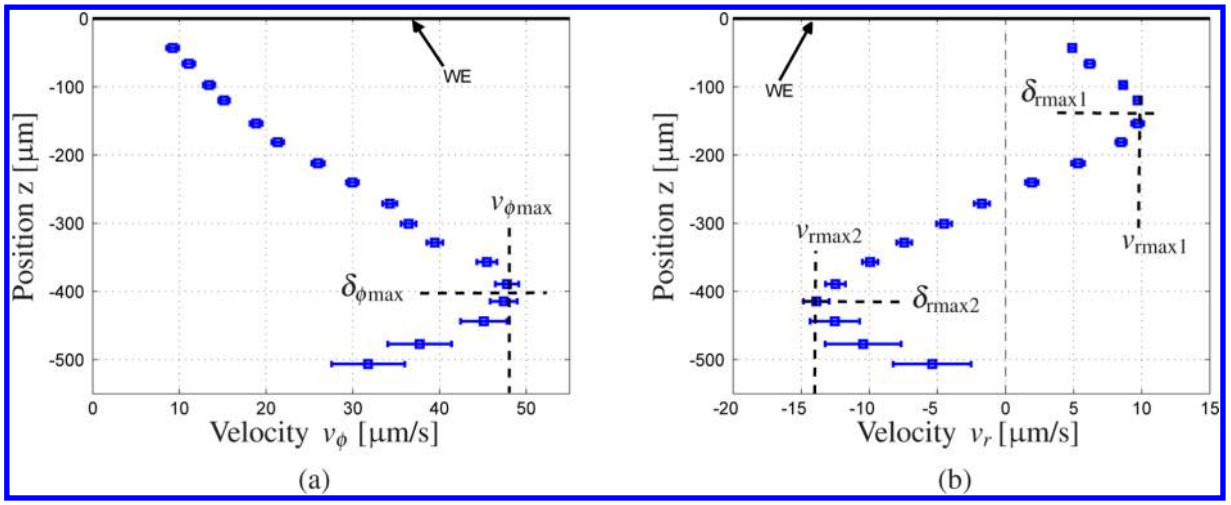

Figure 5. Measured (a) circumferential velocity component and (b) radial velocity component at measurement position r_3 = 1600 μm for a bulk concentration of c_0 = 5 mM. The error bars indicate the standard deviation of the mean velocity values. WE is the working electrode.

as well as on the velocity v_x orthogonal to the fringes. Dividing both Doppler frequencies yields a quotient $q(z)$

$$q(z) = \frac{f_1(v_x, z)}{f_2(v_x, z)} = \frac{v_x/d_1(z)}{v_x/d_2(z)} = \frac{d_2(z)}{d_1(z)} \quad (5)$$

that is independent of the velocity and represents the axial tracer particle position inside the measurement volume. Knowing the actual fringe spacing, $d_1(z)$ and $d_2(z)$, the velocity component $v_x(z)$ is calculated by applying the following:

$$v_x(z) = f_1(v_x, z)d_1(z) = f_2(v_x, z)d_2(z) \quad (6)$$

For details about the LDV-PS, refer to ref 14.

To meet the complexity of the expected electrolyte convection, the LDV-PS has been extended using a third superimposed interference fringe system. With respect to both fringe systems of the LDV-PS, it is turned 90° about the optical z-axis. In addition to the axial tracer particle position and the velocity component $v_x(z)$ of the LDV-PS, it allows the simultaneous determination of the second orthogonal velocity component $v_y(z)$ by applying eq 6 to the corresponding third Doppler frequency f_3.[16] This means for the electrochemical experiment present here, both electrode-parallel velocity components can be measured. Through evaluation of a sufficient number of particles passing through the measurement volume in a statistically distributed manner, the sensor measures the electrode-normal two-component velocity profile inside the concentration boundary layer. With respect to the Fe-wire (see Figure 3), the circumferential $v_\phi(z)$ and the radial $v_r(z)$ velocity component are measured. To suppress reflections from the cathode, chemically inert fluorescent monodispersed polysterene particles (542 nm/612 nm, Duke Scientific Co.) 2 μm in diameter were used as tracer particles. Their density, 1.05 g/cm^3, matches that of the electrolyte.

Measurement Procedure. To show the correlation between the electrolyte convection near the electrode and the deposited structure, four different measurement positions along the centerline of the magnetized Fe-wire were chosen; see Figure 4a. With respect to the symmetrical deposited structure (see Figure 2) and to the radius of the Fe-wire of R = 1 mm in width, the selected lateral measurement positions along the radius are r_1 = 800 μm, r_2 = 1200 μm, r_3 = 1600 μm, and r_4 = 2000 μm away from the Fe-wire center. At each radial measurement position, the electrode-normal two-component velocity profiles were measured with the LDV-PS as follows. The duration of deposition amounted to 600 s. To avoid the strong transients of the initial phase, the velocity measurements were started 60 s later than the electrolysis; see Figure 4b. After this time, steady-state conditions are assumed, meaning that a diffusion layer with a certain concentration gradient Δc has been built up and the magnetic field gradient force can induce additional convection near the electrode, according to eq 3. Furthermore, the deposition is limited by diffusion of Cu^{2+} ions through the diffusion layer and no further significant change of the electrolyte composition occurs. To increase the total number of measurement data (number of tracer particles), the electrolysis was repeated up to five times for each measurement position. To repeat the experiment under almost identical conditions, density stratifications were dissolved after each run by reversing the electrochemical process. To obtain the two-component velocity profiles, all data collected at each measurement position (r_1, r_2, r_3, r_4) were summarized and spatially averaged along the electrode-normal z-axis using a spatial slot of 30 μm in width. Only those increments of length containing at least 10 tracer particles were considered. In this way, the electrode-normal two-component velocity profiles ($v_r(z)$,$v_\phi(z)$) were determined within ≈ 500 μm of the front of the cathode surface at the four different radial measurement positions.

RESULTS AND DISCUSSION

Flow Structure. The electrode-normal two-component velocity profile at measurement position r_3 = 1600 μm is depicted in Figure 5. Following from the no-slip condition, the circumferential velocity component v_ϕ, driven by the Lorentz force density, increases almost linearly with increasing distance to the electrode and reaches its maximum $v_{\phi max}$ at $\delta_{\phi max} \approx -400$ μm in front of the cathode. Similar behavior can be found for the radial velocity component, which reaches its first local maximum at $\delta_{rmax1} \approx -140$ μm . However, with increasing distance to the cathode, the velocity turns and reaches its next local maximum at about $\delta_{rmax2} \approx -415$ μm . This flow pattern, reminiscent of a secondary flow induced in rotating flows, is generally known as Ekman pumping. However, as stated for a similar configuration,[7] the Lorentz force-driven flow cannot induce such a significant secondary flow. Thus, the radial

dx.doi.org/10.1021/ac302601t | Anal. Chem. 2013, 85, 3087−3094

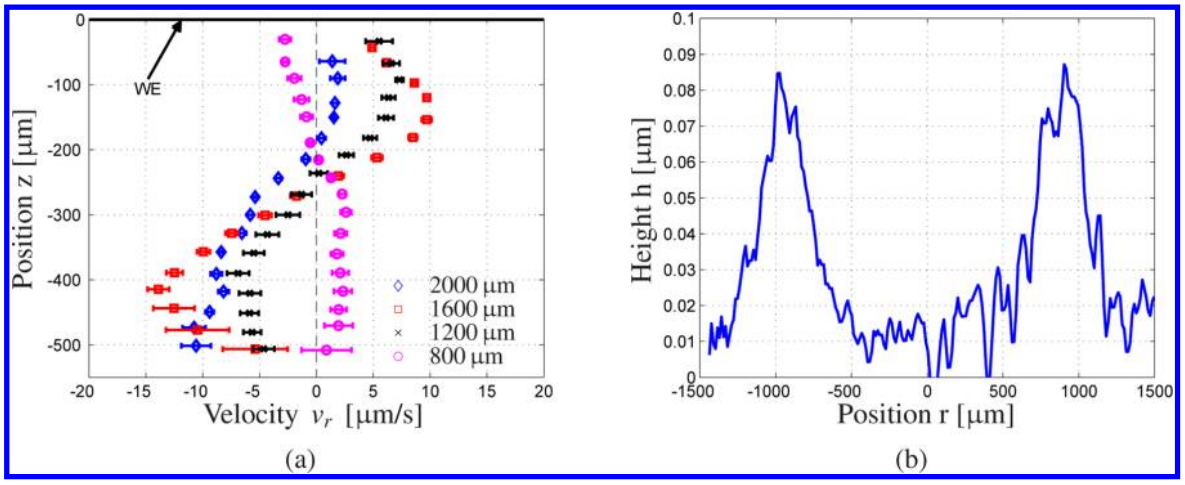

Figure 6. (a) Measured radial velocity component at the four different measurement positions and (b) measured height profile along the centerline of the Fe-wire, c_0 = 5 mM. WE is the working electrode.

velocity component results from the influence of the magnetic field gradient force. According to eq 4, the magnetic field gradient force acts in radial- and electrode-normal direction. As the maximum of $\mathbf{f}_{\nabla B}$ is located at the rim of the Fe-wire, it attracts electrolyte volume containing Cu^{2+} ions particularly toward the rim, both from the radial and electrode-normal direction. The radial velocity profiles at the different measurement positions below the Fe-wire confirm this assumption; see Figure 6a. They show that the electrolyte flows toward the rim of the Fe-wire ($|z| > 200-250$ μm) from the inside as well as from the outside. Because the magnetic field gradient force also acts in electrode-normal direction, a flow impinging the electrode is induced. As a general feature of impinging jets, the flow in direct vicinity of the wall is radially directed outward. Hence, the radial velocity component v_r turns in direct vicinity of the electrode, i.e., within 200 μm of the front of the electrode; see Figure 6a. A stagnation point is, therefore, located near the rim of the Fe-wire. The measured height-profile of the electrodeposit along the centerline of the Fe-wire clearly shows the correlation between electrolyte convection and deposited layer. The profile was analyzed using a chromatic confocal profilometer (MicroProf, company FRT) after a Cu deposition of 10 min duration. The electrolyte convection induced enhances the Cu^{2+} concentration locally and, thus, increases the mass transfer, resulting in higher deposition rates at the rim of the Fe-wire; see Figure 6b.

Considering the circumferential velocity v_ϕ in Figure 7, we note a remarkable behavior. While the velocity profiles at both outer measurement positions (r_3 = 1600 μm, r_4 = 2000 μm) continuously decrease with decreasing distance from the electrode (as generally expected for boundary layer flows), the velocity profiles above the rim (r_1 = 800 μm, r_2 = 1200 μm) exhibit a small plateau and their velocities significantly differ in magnitude. In a first approximation, the reason for this might be explained as follows. As the magnetic field gradient force transports electrolyte-containing Cu^{2+} ions toward the rim, bent current lines result, yielding an electrode-parallel component (j_r) of the current density $\mathbf{j}$, particularly above the rim. In conjunction with the electrode-normal component of the superimposed (homogeneous) magnetic field $\mathbf{B}_{ex}$, the Lorentz force induces additional convection that also stirs azimuthally. Because the sign of the electrode-parallel current density component j_r changes from the inside to the outside of the Fe-wire, the additional convection either supports or opposes the primary Lorentz force-driven convection. Therefore, the total circumferential velocity v_ϕ accelerates and decelerates for the inner (800 μm) and outer (1200 μm) measurement position, respectively.

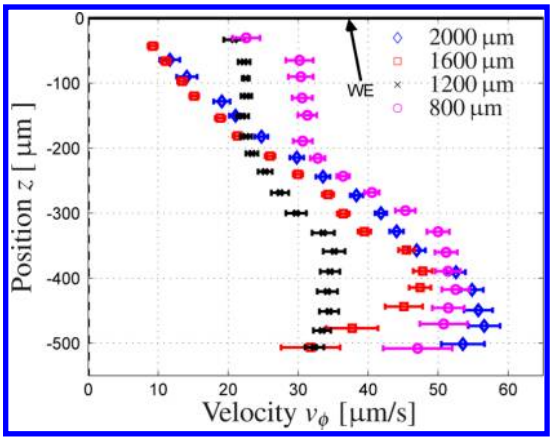

Figure 7. Circumferential velocity component at the four different measurement positions. c_0 = 5 mM. WE is the working electrode.

According to eqs 1 and 2, the higher the concentration c or current density j, the higher the resultant forces. Consequently, faster electrolyte convection is expected when increasing the concentration. In Figure 8, the circumferential and radial velocity profiles at measurement position r_1 = 800 μm are depicted for a concentration of 5 mM and 10 mM. As fewer measurements were conducted for the 10 mM experiment, the uncertainty of the mean velocity values is higher. Nevertheless, for a concentration of 10 mM, we clearly determine a correspondingly higher velocity for both the circumferential and radial component. In accordance with the dependence of the Lorentz force density on the current density (see eq 1), the increase of the maximum circumferential velocity concurs well with the increase of the average limiting current densities measured for both applied concentrations. Furthermore, the general boundary layer flow structure obviously remains. Despite higher velocities, no significant change of the electrode-normal distances ($\delta_{\phi max}$, δ_{rmax1}, δ_{rmax2}) is recognizable. Also, the point where the radial velocity is equal to zero lies nearly at the same position. Furthermore, even the small

dx.doi.org/10.1021/ac302601t | Anal. Chem. 2013, 85, 3087−3094

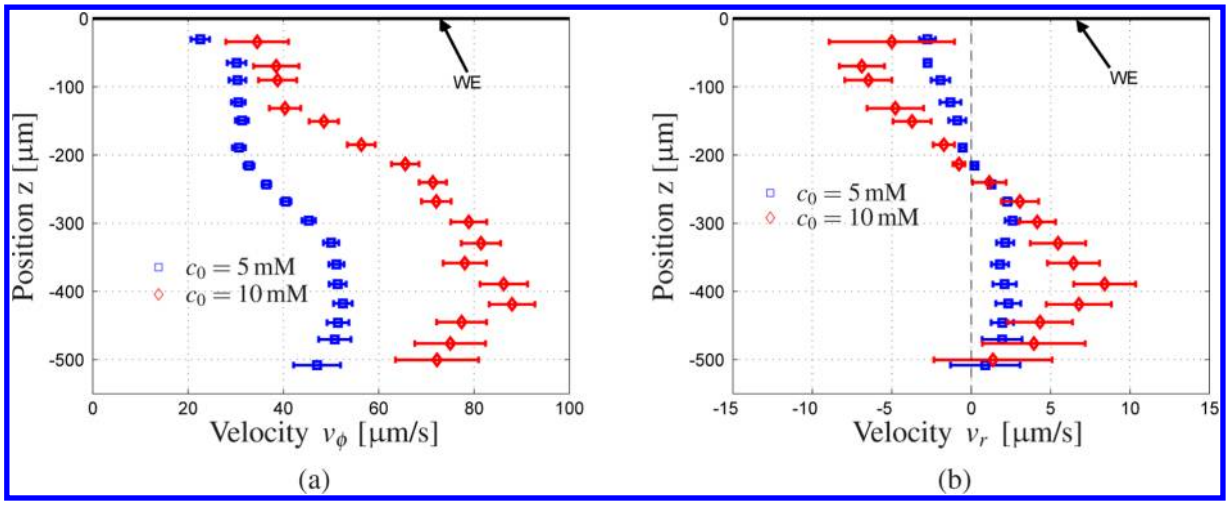

Figure 8. (a) Circumferential and (b) radial velocity profiles at r_1 = 800 μm for a bulk concentration of c_0 = 5 mM and c_0 = 10 mM. WE is the working electrode.

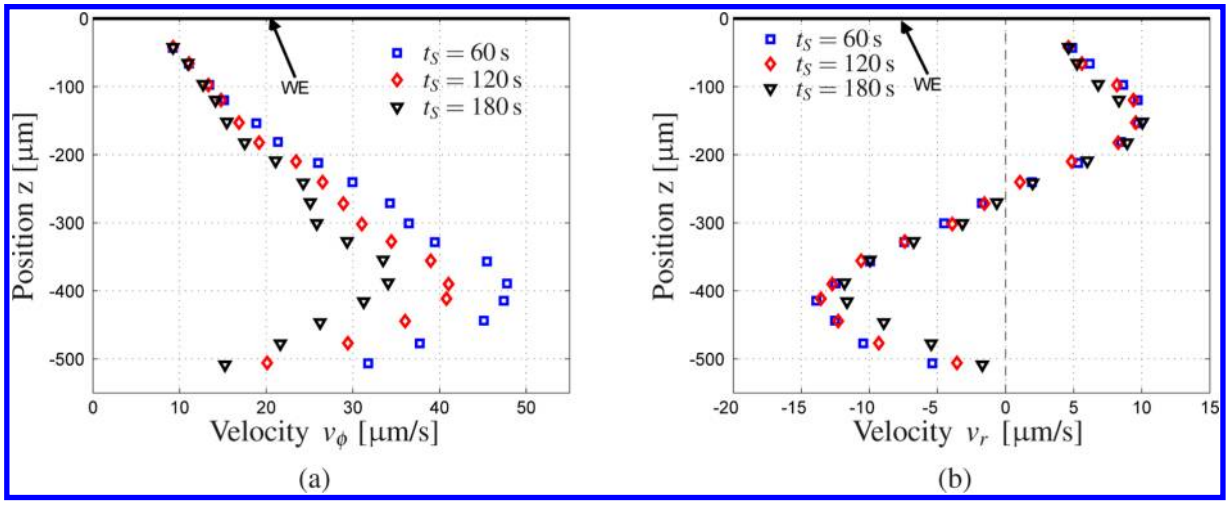

Figure 9. (a) Circumferential and (b) radial velocity profile at measurement position r_3 = 1600 μm for three different starting measurement times t_S = (60, 120, 180) s and a concentration of 5 mM. WE is the working electrode.

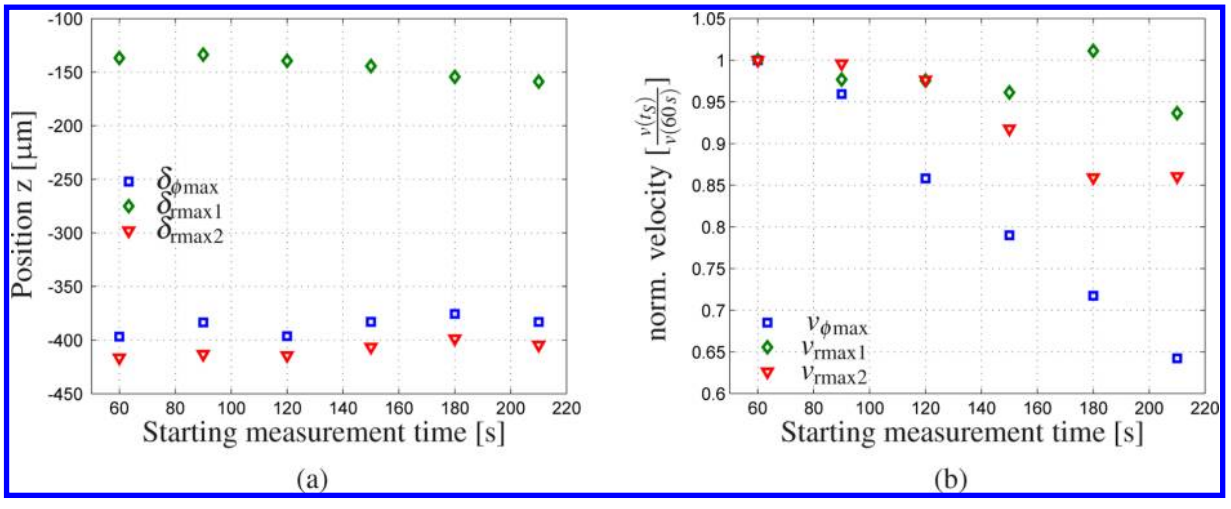

Figure 10. Evolution of (a) the local positions ($\delta_{\phi max}$, δ_{rmax1}, δ_{rmax2}) and (b) the maximum velocities ($v_{\phi max}$, v_{rmax1}, v_{rmax2}) for the different starting measurement times t_S.

plateau of the circumferential velocity is formed in the immediate vicinity of the electrode ($|z|$ < 150 μm).

Transient Behavior. The error bars, which are included in the velocity profiles depicted above, e.g., see Figures 5,

dx.doi.org/10.1021/ac302601t | *Anal. Chem.* 2013, 85, 3087−3094

represent the standard deviation of the mean velocity value at each position. As demonstrated under real flow conditions, the LDV-PS is able to achieve velocity uncertainties in the range of 0.1%.[14] Therefore, the relatively large uncertainty, particularly far away from the electrode, is somewhat surprising. Obviously, the uncertainty mainly originates from the relatively low data rate, on the one hand, and the general measurement procedure, on the other hand. The latter means that uncertainty is increased due to the remaining transient behavior of the flow, even though steady-state conditions are assumed during the measurement time. Therefore, it might be rewarding to analyze the evolution of the velocity boundary layer. As the data rate of the LDV-PS was relatively low, time-resolved velocity profiles are difficult to realize. However, to get a first impression, the evolution of the boundary layer flow is now analyzed by virtually delaying the starting time of the measurement (see Figure 4b) from 60 s (real starting time) until 210 s after starting electrolysis. All data collected before the virtual starting time are ignored. For each measurement time selected, the electrode-normal two-component velocity profiles at measurement position r_3 = 1600 μm are determined by averaging all remaining data along the z-axis using again a spatial slot of 30 μm in width. To visualize the transient behavior of the boundary layer flow, the resulting circumferential and radial velocity components are depicted for three different starting times of the measurement in Figure 9a and Figure 9b, respectively. While the radial flow pattern remains almost constant, we note a significantly decreasing maximum circumferential velocity. This behavior confirms that the radial velocity is indeed not a secondary flow induced by the azimuthally rotating Lorentz force-driven convection, because in that case an equal decrease of both velocities would be expected.

With the six quantities marked in Figure 5, we can analyze the evolution of the boundary layer structure in more detail. Their time dependence is depicted in Figure 10. Obviously, the general flow structure remains almost constant, as no significant change of the local positions ($\delta_{\phi max}$, δ_{rmax1}, δ_{rmax2}) is recognizable; see Figure 10a. However, when comparing the evolution of the maximum velocities ($v_{\phi max}$, v_{rmax1}, v_{rmax2}) in Figure 10b, a significant difference between the circumferential and radial velocity is apparent. Obviously, the circumferential velocity decreases both earlier and faster than the radial velocity. This indicates that the Lorentz and magnetic field gradient force obviously influence the boundary layer flow differently in time.

CONCLUSIONS

Electrolyte convection in the immediate vicinity of the cathode during structured electrodeposition has been measured using an advanced two-component laser Doppler velocity profile sensor (2C-LDV-PS). Three important findings were, for the first time, experimentally revealed.

First, the electrode-normal two-component velocity profiles during Cu deposition in the presence of a magnetized Fe-wire show a significant circumferential as well as radial velocity component inside the concentration boundary layer. Both velocity components are of similar magnitude in the range of a few tens of μm/s at maximum. This confirms the numerically predicted velocity range; see ref 7. The radial velocity component shows that electrolyte convection is induced by the magnetic field gradient force toward the rim of the Fe-wire. This directly correlates to the measured deposited structure using a chromatic confocal profilometric sensor. Due to a transport of Cu^{2+} ions toward the rim of the Fe-wire induced by the forced convection, maximum deposit thicknesses are found there.

Second, the measured velocity profiles, particularly the circumferential velocity component, indicate a more complex boundary layer flow structure as numerically predicted in previous works.[7] Obviously, the Lorentz and magnetic field gradient force are not only superimposed but also affect each other, meaning that the pure presence of competing forces induces additional convection of second order. This applies particularly to the concentration boundary layer, where the magnetic field gradient force is able to induce electrolyte convection. Hence, for future investigations of the mechanism of the structured electrodeposition process, this effect should be considered.

Third, the velocity measurements show a significant transient behavior of the boundary layer flow. By virtually delaying the starting measurement time, the resulting two-component velocity profiles reveal that the influence of the Lorentz force to the boundary layer flow decreases faster than that of the magnetic field gradient force. Despite a significantly decreasing maximum circumferential velocity, the radial flow pattern remains nearly constant during the measurement time. This implies that both forces have different decay constants ($\tau_{f_L} \gg \tau_{f_{\nabla B}}$). In association with the fact that the longer the deposition time, the more pronounced the deposited structure, it proves true that the magnetic field gradient force is mainly responsible for the structuring effect.

AUTHOR INFORMATION

Corresponding Author

*E-mail: Joerg.Koenig@tu-dresden.de; K.Tschulik@ifw-dresden.de.

Notes

The authors declare no competing financial interest.

ACKNOWLEDGMENTS

The authors thank K. Eckert, G. Mutschke, and T. Weier for very fruitful discussions and comments. Funding by the German Research Foundation through the Collaborative Research Center (SFB) 609 (parts A8 and C6) is gratefully acknowledged.

REFERENCES

(1) Weston, M. C.; Gerner, M. D.; Fritsch, I. *Anal. Chem.* **2010**, *82*, 3411−3418.

(2) Leventis, N.; Gao, X. *Anal. Chem.* **2001**, *73*, 3981−3992.

(3) Ragsdale, S. R.; Grant, K. M.; White, H. S. *J. Am. Chem. Soc.* **1998**, *120*, 13461−13468.

(4) Leventis, N.; Gao, X. *J. Am. Chem. Soc.* **2002**, *124*, 1079−1088.

(5) Tschulik, K.; Koza, A., J.; Uhlemann, M.; Gebert, A.; Schultz, L. *Electrochem. Commun.* **2009**, *11*, 2241−2244.

(6) Tschulik, K.; Sueptitz, R.; Koza, J.; Uhlemann, M.; Mutschke, G.; Weier, T.; Gebert, A.; Schultz, L. *Electrochim. Acta* **2010**, *56*, 297−304.

(7) Mutschke, G.; Tschulik, K.; Weier, T.; Uhlemann, M.; Bund, A.; Fröhlich, J. *Electrochim. Acta* **2010**, *55*, 9060−9066.

(8) Tschulik, K.; Cierpka, C.; Anett, G.; Schultz, L.; Kähler, C.; Uhlemann, M. *Anal. Chem.* **2011**, *83*, 3275−3281.

(9) Tschulik, K.; Sueptitz, R.; Uhlemann, M.; Schultz, L.; Gebert, A. *Electrochim. Acta* **2011**, *56*, 5174−5177.

(10) Dunne, P.; Coey, J. M. D. *Phys. Rev. B* **2012**, *85*, 224411.

(11) Brett, C. M. A.; Oliveira Brett, A. M. *Electrochemistry: Principles, Methods, and Applications*, 1st ed.; Oxford University Press: New York, 1993.
(12) Hamann, C. H.; Hamnett, A.; Vielstich, W. *Electrochmistry*, 2nd ed.; Wiley-VCH: Weinheim, 2007.
(13) Lide, R. D. *Handbook of Chemistry and Physics*, 84th ed.; CRC Press: Boca Raton, FL, 2003.
(14) König, J.; Voigt, A.; Büttner, L.; Czarske, J. *Meas. Sci. Technol.* **2010**, *21* (9), 074005.
(15) König, J.; Mühlenhoff, S.; Kerstin, E.; Büttner, L.; Odenbach, S.; Czarske, J. *Electrochim. Acta* **2011**, *56*, 6150−6156.
(16) Albrecht, H. E.; Borys, M.; Damaschke, N.; Tropea, C. *Laser Doppler and Phase Doppler Measurement Techniques*; Springer: New York, 2003.